Journal of Modern Optics

ISSN: 0950-0340 (Print) 1362-3044 (Online) Journal homepage: http://www.tandfonline.com/loi/tmop20

Ultrafast optical Kerr gate imaging in a poly-disperse turbid medium

Yuhu Ren, Wenjiang Tan, Jinhai Si, Shichao Xu, Junyi Tong & Xun Hou

To cite this article: Yuhu Ren, Wenjiang Tan, Jinhai Si, Shichao Xu, Junyi Tong & Xun Hou (2016) Ultrafast optical Kerr gate imaging in a poly-disperse turbid medium, Journal of Modern Optics, 63:6, 513-518, DOI: 10.1080/09500340.2015.1083128

To link to this article: http://dx.doi.org/10.1080/09500340.2015.1083128

Published online: 02 Sep 2015.

Journal of Modern Optics, 2016
Vol. 63, No. 6, 513–518, http://dx.doi.org/10.1080/09500340.2015.1083128

Ultrafast optical Kerr gate imaging in a poly-disperse turbid medium

Yuhu Ren[a], Wenjiang Tan[a]*, Jinhai Si[a], Shichao Xu[a], Junyi Tong[b] and Xun Hou[a]

[a]*Key Laboratory for Physical Electronics and Devices of the Ministry of Education & Shaanxi Key Lab of Information Photonic Technique, Collaborative Innovation Center of Suzhou Nano Science and Technology, School of Electronics & Information Engineering, Xi'an Jiaotong University, Xi'an, China;* [b]*Departments of Applied Physics, Xi'an University of Technology, Xi'an, China*

(*Received 2 March 2015; accepted 10 August 2015*)

The influence of the size parameter of the scatterers on ultrafast optical Kerr gate (OKG) imaging is investigated in highly scattering poly-disperse turbid media. The results show that in a poly-disperse turbid medium, which in our case, is a suspension of two different sized mono-disperse microspheres, the temporal and spatial behaviors of the light pulses transmitted through it are dominated by the smaller microspheres. The contrasts of the OKG images for the poly-disperse microsphere sample are closer to the contrasts of the OKG images for the smaller sized mono-disperse microsphere sample.

Keywords: optical Kerr gate; ballistic imaging; poly-disperse turbid medium; Mie scattering; femtosecond laser

1. Introduction

The propagation of light in randomly scattering media such as clouds [1], fogs [2], or aerated spray [3,4] has received increasing interest. One major motivation for this study is the potential for applying optical imaging to objects hidden in the scattering medium [5]. The diffuse photons deteriorate the imaging resolution, and reducing this deterioration is the main challenge associated with optical imaging. Thanks to femtosecond lasers and techniques such as second harmonic generation imaging [6] or optical Kerr gate (OKG) imaging [7,8], it is possible to obtain the imaging of objects hidden in a turbid medium. OKG imaging has been used to enhance the contrast between these objects and the background since the multiply scattered photons can be removed by time gating [9,10].

The OKG imaging in a turbid medium is influenced by the scattering properties of the turbid medium, i.e., the scattering coefficient and the anisotropy parameter [11,12]. Earlier studies [13–17] in the optical imaging of a turbid medium have shown that the size parameter, the shape, and the refractive index of the scatterer have an impact on the spatial resolution of images. Another important factor that could contribute to the image contrast of the OKG image is the arrangement of OKG. The influence of the OKG on the image contrast for different Kerr media has been investigated [18,19]. The results show that the OKG of large optical nonlinearity Kerr material can provide high-contrast images. Most of the studies mentioned above focus on the optical imaging in the mono-disperse scattering medium. However, in many practical situations [20,21], it is necessary to deal with the OKG imaging in poly-disperse turbid media with higher concentrations. In the previous investigations, Velazco-Roa et al. presented a method to extract the complex refractive [22] index of spherical particles from a poly-disperse turbid medium. Ghosh described the effect of a distribution in the size of scatterers on the depolarization of light in turbid media at low optical depth (OD) [23].

In this paper, we investigate the influence of the size parameter of the scatterer on OKG imaging in highly scattering poly-disperse turbid medium. The OKG images for the poly-disperse sample and the temporal characteristic of the light transmitted through the poly-disperse turbid medium are obtained. The experimental results show that the contrasts of the OKG images for the poly-disperse turbid medium having a mixture of two different sized mono-disperse silica microspheres suspension by volume ratio (1:1) are mainly influenced by the smaller microsphere of the two microspheres. In addition, the temporal characteristic of the laser pulses transmitted through the poly-disperse turbid medium is dominated by the smaller sized microspheres.

2. Experiment setup

The schematic of the OKG imaging system is shown in Figure 1. A Ti: sapphire laser was used to provide 800 nm light pulses with a full width at half maximum (FWHM) of 50 fs and a repetition rate of 1 kHz. The laser beam was split into a gating beam centered at

*Corresponding author. Email: tanwenjiang@mail.xjtu.edu.cn

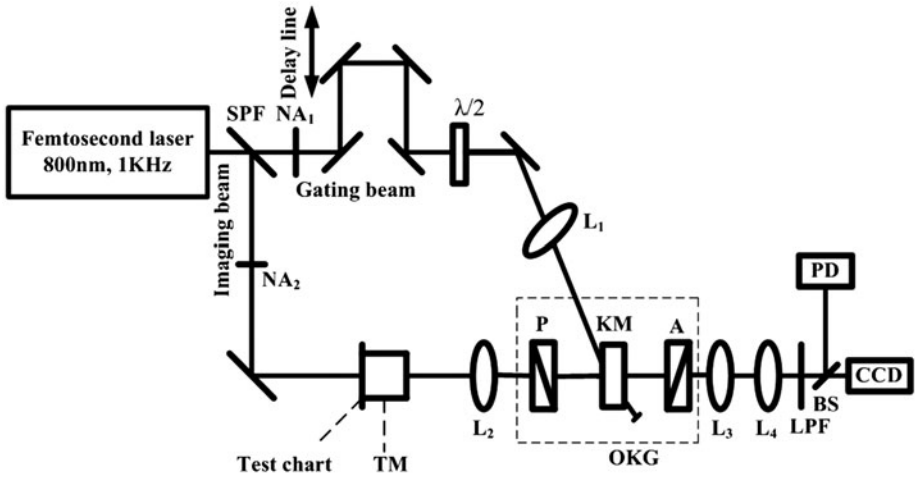

Figure 1. Experimental setup for the OKG imaging system. L: lens; SPF: short-pass filter; λ/2: half-wave plate; P: polarizer; A: analyzer; NA: neutral attenuator; LPF: long-pass filter; TM: turbid medium; KM: Kerr medium; BS: beam splitter; OKG: optical Kerr gate.

780 nm and an imaging beam centered at 800 nm by a short-pass filter (SPF). The gating beam was used to trigger the optical Kerr gate and the imaging beam was used as the illumination source. The power of the gating or imaging beam was adjusted by neutral attenuators (NA_1 and NA_2). The imaging beam was first modulated by a 1.41-line-pair/mm resolution chart (a chromium-coated glass US Air Force resolution chart) and then introduced to the turbid medium. The transmitted light from the turbid medium was directed to the OKG, which enables sampling of either the ballistic or the scattered light by adjusting the delay between the pump and probe pulses. The first polarizer of the OKG was set parallel and the second one was set perpendicular to the polarization of the imaging beam. Then, the imaging beam was split into two separated branches detected by a charge-coupled device camera and a photo diode, respectively. The polarization of the gating beam was done using a half-wave (λ/2) plate and was first linear, at 45° with respect to the polarization of the imaging beam for optimal efficiency. Thereafter, the gating beam was focused into the Kerr medium of CS_2 filled in a 5-mm quartz cell and then passed to the ultrafast OKG imaging in the turbid medium. A long-pass filter (LPF) was placed before the beam splitter (BS) to block noise light caused by the gating beam scattering forward into the detecting devices.

The turbid medium was composed of a silica microsphere solution contained in a cubic cuvette with inside dimensions of 50 mm × 50 mm × 10 mm. The thickness of the cuvette along the optical axis was 10 mm. The diameters of the silica microspheres were 0.43 and 3.07 μm. The refractive indices of the background medium n_b and the silica microspheres n_p were 1.33 and 1.45, respectively. The absorption of the turbid medium was low enough to be ignored. The poly-disperse microsphere suspension was prepared using a 1:1 volume ratio mixture of 0.43 μm diameter microspheres and 3.07 μm diameter microspheres suspensions, both having an optical depth OD = 8.5. This ensured that the mixtures of the two suspensions also had a value of OD = 8.5. The optical density (OD) of the each microsphere suspension was varied by changing the scattering coefficient μ_s of the samples by dilution. The two mono-disperse microsphere suspensions are also used as reference samples.

3. Results and discussion

The OKG imaging method enhances the image contrast by temporally limiting the collection of scattered

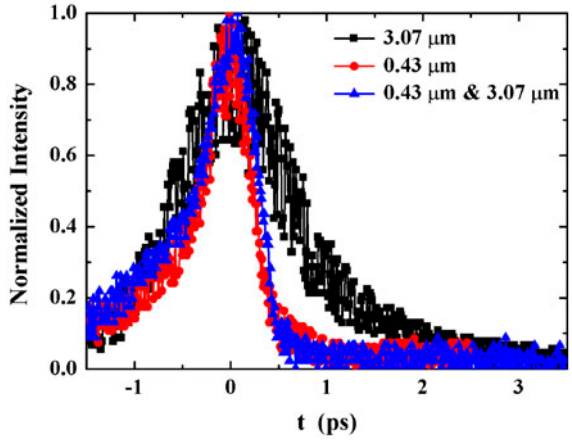

Figure 2. Normalized-intensity temporal profiles of the light pulses through the three different samples. (The colour version of this figure is included in the online version of the journal.)

photons. Therefore, it is helpful to understand the temporal character of the light pulses through the turbid media. Figure 2 shows the normalized intensity temporal profiles of the light pulses transmitted through the poly-disperse microsphere suspension, which were obtained using OKG. The temporal profiles of the light pulses transmitted through the two mono-disperse microsphere suspensions are also shown in Figure 2 as reference signals. The zero time was taken to be the instant when the ballistic photons entered the photo diode. The scattered photons followed the ballistic photons and appeared at the positive delay time. It can be seen from Figure 2 that there is only one distinct ballistic peak at the time $t = 0$ ps for each microsphere suspension. Whereas, the width of the light pulses transmitted through each microsphere suspension is different. The FWHM of the light pulses transmitted through the larger sized microsphere suspension is approximately 1.5 ps. The FWHM of the light pulses transmitted through the smaller sized microsphere suspension is about 0.8 ps. Further, it can also be seen that the temporal profile of the light pulses transmitted through the poly-disperse microsphere sample is closer to that of the light pulses transmitted through the smaller sized microsphere suspension.

In order to examine the effect of the characteristics of the turbid medium on the image quality, the images of the test chart hidden in different silica microsphere samples are shown in Figure 3. In Figure 3(*a*), we show the direct imaging for the sample filled with deionized water without using OKG as the reference image. In Figure 3(*b*) and (*c*), we show the direct imaging and the OKG imaging for the larger sized microsphere sample, respectively. It can be seen that the OKG imaging enhances the contrast between the target and its background. The decrease in the boundary sharpness of the OKG image here is due to the low-pass spatial filtering effect of the OKG [7].The OKG imaging for the smaller sized microsphere sample is shown in Figure 3(*d*). The corresponding result for the poly-disperse microsphere sample A is shown in Figure 3(*e*). Figures 3(*c*)–(*e*) indicate that the visualization of the OKG imaging for the poly-disperse microsphere sample is closer to that for the smaller sized microsphere suspension.

To quantitatively evaluate the performance of the OKG imaging system, we measured the modulation transfer function (MTF) of the OKG imaging system for the three different microsphere suspensions. The MTF is given by $\mathrm{MTF}(f) = C(f)/C_0(f)$, where the image contrast is defined as $C(f) = (I_{\max} - I_{\min})/(I_{\max} + I_{\min})$. Further, $C_0(f)$ denotes the modulation of the object, f is the spatial frequency. The image contrast is calculated using the average light intensity retrieved from the dark region ($I_{\min}$) and the average light retrieved from the unshadowed region ($I_{\max}$) of the test chart. From Figure 4, we see that the maximum resolvable spatial frequencies of OKG imaging system are 7.3 line pairs per millimeter (lp/mm) for the three different microsphere suspensions. However, at different spatial frequencies, the contrasts of the images for the smaller sized microsphere sample are higher than those of the images for the larger sized microsphere suspension.

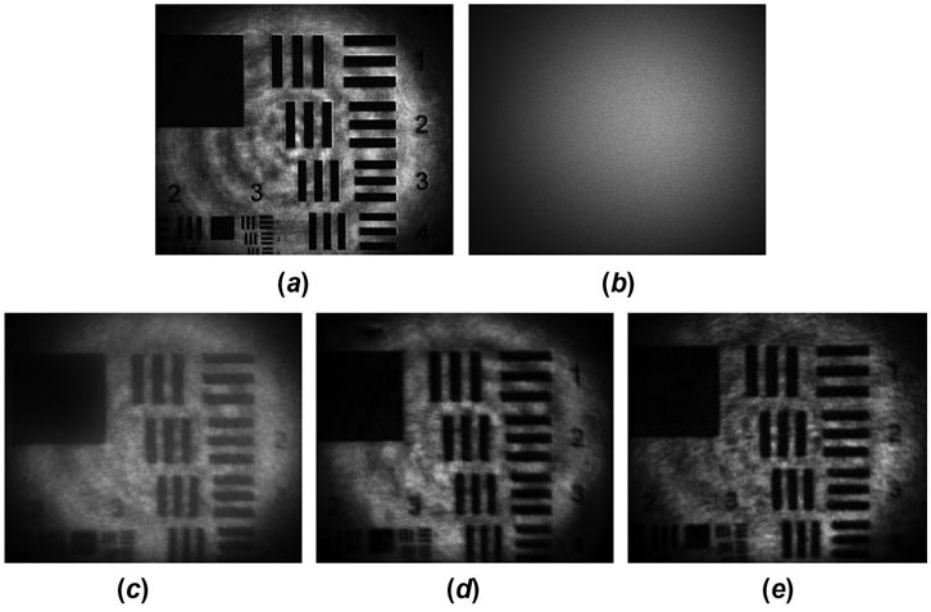

Figure 3. Images of the test chart hidden in different silica microsphere samples. (*a*) reference image, (*b*) no time gate (standard transillumination), (*c*) images for the larger sized microsphere sample using OKG, (*d*) images for the smaller sized microsphere sample using OKG, (*e*) images for the poly-disperse microsphere sample using OKG.

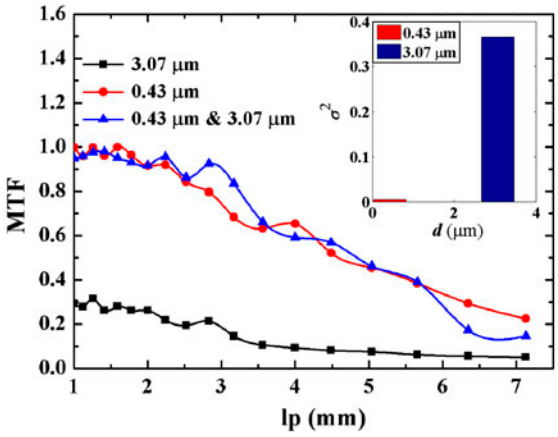

Figure 4. MTF of the OKG imaging system for different microsphere samples and the overall standard deviations (σ^2) between different MTF curves of the OKG imaging system for different microsphere suspensions. (The colour version of this figure is included in the online version of the journal.)

Further, the spatial contrast of the OKG imaging for the poly-disperse microsphere sample is closer to that of the OKG images for the smaller sized microsphere sample. Quantitatively, we calculate the overall standard deviation (σ^2) between different MTF curves using the equation $\sigma^2 = \frac{1}{N-1}\sum_{i=1}^{N}(g(f_i) - h(f_i))^2$, where $g(f)$ and $h(f)$ are the different MTF curves for the poly-disperse sample and the mono-disperse suspension, respectively. N is the number of the sampling points of MTF curves. The overall standard deviations between different MTF curves are shown in the inset of Figure 4. It can be seen that the overall standard deviation between MTF curves for the poly-disperse microsphere sample and the smaller mono-disperse suspension is 0.005, but that for the poly-disperse microsphere sample and the larger mono-disperse suspension is 0.366. The result further confirms that the spatial contrast of the OKG imaging system for the poly-disperse microsphere sample is closer to that of the OKG images for the smaller sized microsphere suspension.

To explain the experimental results shown above, we further analyzed the scattering efficiency (Q) and the scattering phase function $p(\theta)$ of the two diameter microspheres. The scattering efficiency and the scattering phase functions computed using Mie theory [24] are shown in Figure 5. From Figure 5(a), we can see that the scattering efficiency of the smaller sized microsphere (0.43 μm) is 0.84, while the efficiency of the larger sized microsphere (3.07 μm) is 2.82. Further, in our experiment, the collection angle of the OKG system is approximately 8°. According to the formula $Q_r = \frac{\int_0^8 p(\theta)\mathrm{d}\theta}{\int_0^{180} p(\theta)\mathrm{d}\theta}$, the forward scattering efficiency of the microsphere can be obtained. It can be seen from Figure 6(b) that the forward scattering intensity of the larger sized microsphere suspension is higher than that of the smaller sized microsphere suspension. The forward scattering ability $Q_r\pi(d/2)^2$ of the larger sized microsphere is about 18 times that of the smaller sized microsphere. Furthermore, in the small collection angle, most of the scattered photons from the turbid medium are the early arriving photons that have traveled over the shorter path. In our experiment, the switching time of the OKG of CS_2 is approximately 1.5 ps. During the switching time, the intensity of the residual scattered light of a larger sized microsphere passed through the OKG is higher than that of the residual scattered light of a smaller sized microsphere. Hence, the temporal and spatial characteristics of the light transmitted through the poly-disperse sample should be closer to those of the light transmitted through the larger sized microsphere suspension. However, discrepancy is observed in the normalized intensity temporal profiles of the light pulses through the three different suspensions in Figure 2. Discrepancy is also observed in the MTF of the OKG imaging for the three different microsphere samples shown in Figure 4.

Considering the mono-disperse microsphere particles, the optical depth ($\mathrm{OD} = n{\cdot}\sigma{\cdot}L$) derived from the Beer–Lambert law relates to the particle scattering cross section σ, the number density n and the path length L. The scattering cross section is a function of the diameter of the microsphere and is given by $\sigma = Q\pi(d/2)^2$ [25]. Under the same OD condition, the total scattering ability ($n{\cdot}\sigma$) of the microsphere suspension with smaller sized microspheres is equal to that of the microsphere suspension with larger sized microspheres. Since the poly-disperse microsphere sample was prepared using 1:1 volume ratio mixture of the two mono-disperse suspensions, the number density of the sample with smaller sized microsphere suspension is about 2000 times that of the sample with larger sized microsphere suspension in poly-disperse microsphere sample. Hence, the total forward scattering ability $nQ_r\pi(d/2)^2$ of the smaller sized microspheres is about 110 times that of the larger sized microspheres in the poly-disperse microsphere sample. The temporal and spatial characteristics of the light transmitted through the poly-disperse microsphere sample should thus be dominated by the smaller sized microsphere. It should be noted here that although the single-scattering theoretical treatment presented above does show qualitative agreement with the experimental results, a quantitative evaluation would require the inclusion of the effect of multiple scattering.

In addition, to identify whether the similar results can be obtained for the poly-disperse microsphere samples with other particle sizes, we performed the OKG imaging in other poly-disperse samples. The

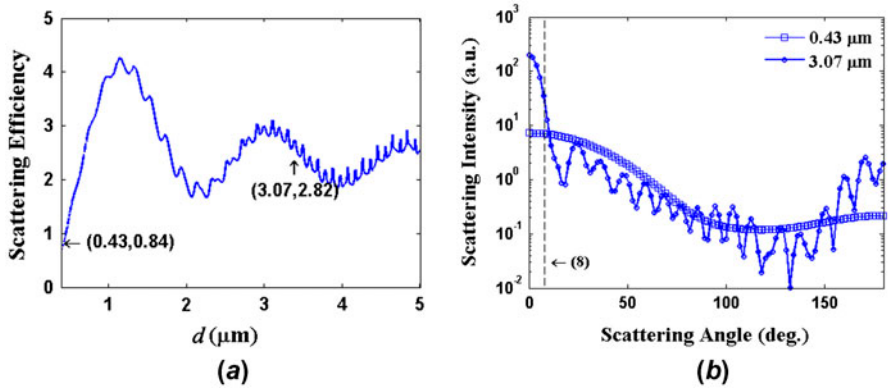

Figure 5. (*a*) Scattering efficiency vs. diameter for a silica microsphere; (*b*) Scattering phase function with $d = 0.43$ μm (squares) and $d = 3.07$ μm (circles). (The colour version of this figure is included in the online version of the journal.)

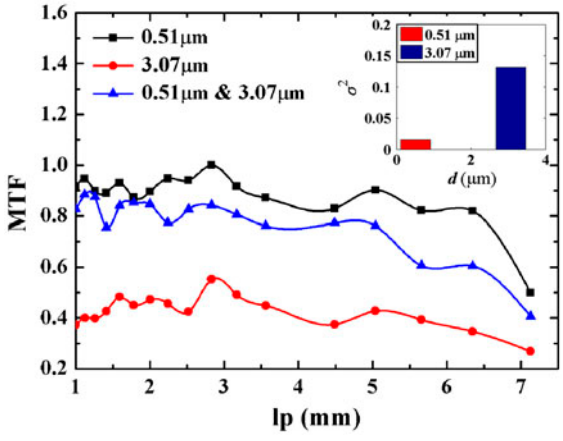

Figure 6. MTF of the spatial gated imaging for different microsphere suspensions and the overall standard deviations (σ^2) between different MTF curves of the spatial gated imaging system for the poly-disperse microsphere suspension and mono-disperse suspension. (The colour version of this figure is included in the online version of the journal.)

Table 1. Characteristics of the poly-disperse microsphere samples.

Sample	Particle diameters (μm)	Volume ratio
A	0.51:3.07	1:1
B	0.43:5.65	1:1
C	3.07:5.65	1:1

characteristics of the poly-disperse microsphere samples are shown in Table 1. Similar results for the temporal and spatial behaviors of the light pulses transmitted through three different poly-disperse microsphere samples have been observed. Here, we show the overall standard deviations between MTF curves of the OKG imaging for the different poly-disperse microsphere samples and the mono-disperse microsphere suspensions. From Table 2, we can see that the overall standard deviations between MTF curves of the OKG imaging for the poly-disperse microsphere samples and the smaller mono-disperse suspensions are smaller. The results indicate that the spatial contrasts of the OKG imaging for the poly-disperse microsphere samples are also closer to those of the OKG images for the smaller sized microsphere suspensions for these samples with other particle sizes.

To identify whether the similar experimental results as described above can be obtained using other methods, we also performed the spatial-gated imaging as a comparative experiment. Figure 6 shows the MTF of the spatial-gated imaging for the three different microsphere suspensions. In the spatial-gated imaging experiment, the Kerr medium was replaced with an aperture which was placed at the back focal plane of lens L_2. The diameter of the aperture was 2 mm. The polarizer and analyzer were removed, and the gating beam was also blocked. The sample *A* was chosen as the poly-disperse microsphere suspension. From Figure 6, we can see that the spatial contrast of the spatial-gated imaging for the poly-disperse microsphere sample is closer to that for the smaller sized microsphere suspension. As shown in the inset of Figure 6, the overall standard deviations between MTF curves of the spatial-gated imaging for the poly-disperse microsphere sample and the smaller mono-disperse suspension is 0.015, but that for the poly-disperse microsphere sample and the larger mono-disperse suspension is 0.131. The experimental results show that the contrast of the spatial-gated imaging for the poly-disperse microsphere sample is closer to that for the smaller sized mono-disperse microsphere suspension, which is similar to the results obtained using the OKG imaging.

Table 2. Overall standard deviations (σ^2) between different MTF curves of the OKG imaging for the poly-disperse microsphere suspensions and mono-disperse suspensions.

Sample	Mono-disperse microsphere suspension	Overall standard deviation
A	0.51	0.020
	3.07	0.133
B	0.43	0.009
	5.65	0.113
C	3.07	0.132
	5.65	0.241

4. Conclusion

In summary, we investigated the influence of the size parameter of the scatterer on ultrafast optical Kerr gate (OKG) imaging in a poly-disperse turbid medium having a mixture of suspension of mono-disperse silica microspheres of two different sizes by volume ratio (1:1). We compared the temporal and spatial behaviors of light pulses transmitted through the poly-disperse turbid medium with those of light pulses transmitted through the mono-disperse turbid medium. The results show that of the two microsphere samples, the temporal behavior of transmitted light through the poly-disperse turbid medium is dominated by the smaller sized microspheres. Further, the contrasts of the OKG images for the poly-disperse turbid medium are closer to the contrasts of the OKG images for the smaller sized microsphere suspension.

Disclosure statement

No potential conflict of interest was reported by the authors.

Funding

This work was supported by the National Natural Science Foundation of China [grant number 61235003], [grant number 61427816], [grant number 61308036], [grant number 61205129]; the China Postdoctoral Science Foundation funded project [grant number 2013M540753]; collaborative innovation center of Suzhou nano science and technology.

References

[1] Zege, E.P.; Katsev, L.L.; Polonsky, I.N. *J. Appl. Opt*. **1993,** *32,* 2803–2812.
[2] Mahalati, R.N.; Kahn, J.M. *J. Opt. Express* **2012,** *20,* 1649–1661.
[3] Sedarsky, D.; Gord, J.; Carter, C.; Meyer, T.; Linne, M. *J. Opt. Lett*. **2009,** *34,* 2748–2750.
[4] Idlahcen, S.; Rozé, C.; Méès, L.; Girasole, T.; Blaisot, J.B. *J. Exp. Fluids* **2012,** *52,* 289–298.
[5] Wang, L.; Ho, P.P.; Liu, C.; Zhang, G.; Alfano, R.R. *J. Sci.* **1991,** *253,* 769–771.
[6] Ambekar, R.; Lau, T.Y.; Walsh, M.; Bharqava, R.; Toussaint, K.C. *J. Biomed Opt. Express* **2012,** *3,* 2021–2035.
[7] Wang, L.; Ho, P.P.; Liang, X.; Dai, H.; Alfano, R.R. *J. Opt. Lett*. **1993,** *18,* 241–243.
[8] Wang, L.; Ho, P.P.; Alfano, R.R. *J. Appl. Opt*. **1993,** *32,* 5043–5048.
[9] Zhan, P.P.; Tan, W.J.; Si, J.H.; Xu, S.C.; Tong, J.Y.; Hou, X. *J. Appl. Phys. Lett*. **2014,** *104,* 211907.
[10] Idlahcen, S.; Méès, L.; Rozé, C.; Girasole, T.; Blaisot, J.B. *J. Opt. Soc. Am. A*. **2009,** *26,* 1995–2004.
[11] Bartlett, M.A.; Jiang, H. *J. Appl. Opt*. **2001,** *40,* 1735–1741.
[12] Levitz, D.; Thrane, L.; Frosz, H.M.; Andersen, P.E. *J. Opt. Express* **2004,** *12,* 249–259.
[13] Shukla, P.; Pradhan, A. *J. Appl. Opt*. **2009,** *48,* 6099–6104.
[14] Shukla, P.; Sumathi, R.; Gupta, S.; Pradhan, A. *J. Opt. Soc. Am. A*. **2007,** *24,* 1704–1713.
[15] Bicout, D.; Brosseau, C.; Martinez, A.S.; Schmitt, J.M. *J. Phys. Rev. E.* **1994,** *49,* 1767–1770.
[16] Cheng, T.H.; Gu, X.F.; Yu, T.; Tian, G.L. *J. Quan. Spectrosc. Radiat*. **2010,** *111,* 895–906.
[17] Ghosh, N.; Pradhan, A.; Gupta, P.K.; Gupta, S.; Jaiswal, V.; Singh, R.P. *J. Phys. Rev. E*. **2004,** *70,* 066607.
[18] Zhan, P.P.; Tan, W.J.; Liu, X.; Wu, B.; Si, J.H.; Chen, F.; Hou, X. *J. Opt*. **2013,** *15,* 055202.
[19] Tan, W.J.; Zhou, Z.G.; Lin, A.X.; Si, J.H.; Zhan, P.P.; Wu, B.; Hou, X. *J. Opt. Express* **2013,** *21,* 7740–7747.
[20] Sedarsky, D.; Berrocal, E.; Linne, M. ICLASS. Proceedings of the 11th Triennial International Annual Conference on Liquid Atomization and Spray Systems, Vail, CO, USA, July, 2009.
[21] Scott, D.M. *J. Part. Part. Syst. Charact.* **2003,** *20,* 305–310.
[22] Velazco-Roa, M.A.; Thennadil, S.N. *J. Appl. Opt*. **2007,** *46,* 3730–3735.
[23] Ghosh, N.; Patel, H.; Gupta, P. *J. Opt Express* **2003,** *11,* 2198–2205.
[24] Van de Hulst, H.C. *Light Scattering by Small Particles*; Wiley: New York, 1957; p 263.
[25] Payri, F.; Pastor, J.V.; Payri, R.; Manin, J. *Mech. Sci. Technol.* **2011,** *25,* 209–219.